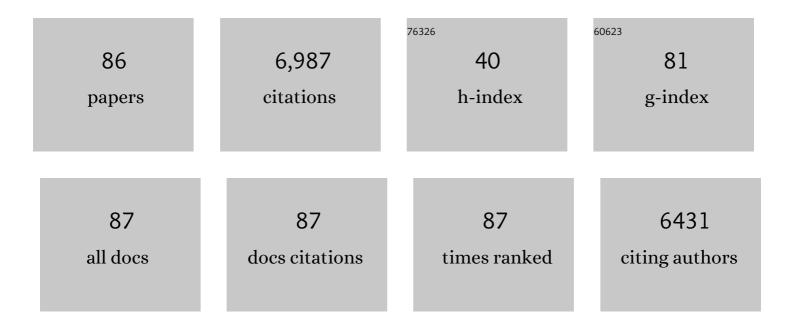
List of Publications by Year in descending order

Source: https://exaly.com/author-pdf/4876440/publications.pdf

Version: 2024-02-01



#	Article	IF	CITATIONS
1	Spatiotemporal characteristics, patterns, and causes of land-use changes in China since the late 1980s. Journal of Chinese Geography, 2014, 24, 195-210.	3.9	1,248
2	Mapping paddy rice planting area in northeastern Asia with Landsat 8 images, phenology-based algorithm and Google Earth Engine. Remote Sensing of Environment, 2016, 185, 142-154.	11.0	524
3	A global moderate resolution dataset of gross primary production of vegetation for 2000–2016. Scientific Data, 2017, 4, 170165.	5.3	335
4	A mangrove forest map of China in 2015: Analysis of time series Landsat 7/8 and Sentinel-1A imagery in Google Earth Engine cloud computing platform. ISPRS Journal of Photogrammetry and Remote Sensing, 2017, 131, 104-120.	11.1	288
5	Tracking the dynamics of paddy rice planting area in 1986–2010 through time series Landsat images and phenology-based algorithms. Remote Sensing of Environment, 2015, 160, 99-113.	11.0	257
6	Mapping paddy rice planting areas through time series analysis of MODIS land surface temperature and vegetation index data. ISPRS Journal of Photogrammetry and Remote Sensing, 2015, 106, 157-171.	11.1	207
7	Divergent trends of open-surface water body area in the contiguous United States from 1984 to 2016. Proceedings of the National Academy of Sciences of the United States of America, 2018, 115, 3810-3815.	7.1	199
8	Mapping cropping intensity in China using time series Landsat and Sentinel-2 images and Google Earth Engine. Remote Sensing of Environment, 2020, 239, 111624.	11.0	187
9	Consistency between sun-induced chlorophyll fluorescence and gross primary production of vegetation in North America. Remote Sensing of Environment, 2016, 183, 154-169.	11.0	180
10	Carbon loss from forest degradation exceeds that from deforestation in the Brazilian Amazon. Nature Climate Change, 2021, 11, 442-448.	18.8	166
11	Open Surface Water Mapping Algorithms: A Comparison of Water-Related Spectral Indices and Sensors. Water (Switzerland), 2017, 9, 256.	2.7	147
12	Tracking annual changes of coastal tidal flats in China during 1986–2016 through analyses of Landsat images with Google Earth Engine. Remote Sensing of Environment, 2020, 238, 110987.	11.0	146
13	Satellite-observed pantropical carbon dynamics. Nature Plants, 2019, 5, 944-951.	9.3	141
14	Mapping coastal wetlands of China using time series Landsat images in 2018 and Google Earth Engine. ISPRS Journal of Photogrammetry and Remote Sensing, 2020, 163, 312-326.	11.1	138
15	Spatiotemporal patterns of paddy rice croplands in China and India from 2000 to 2015. Science of the Total Environment, 2017, 579, 82-92.	8.0	127
16	Mapping paddy rice planting area in cold temperate climate region through analysis of time series Landsat 8 (OLI), Landsat 7 (ETM+) and MODIS imagery. ISPRS Journal of Photogrammetry and Remote Sensing, 2015, 105, 220-233.	11.1	118
17	Continued decrease of open surface water body area in Oklahoma during 1984–2015. Science of the Total Environment, 2017, 595, 451-460.	8.0	118
18	Mapping sugarcane plantation dynamics in Guangxi, China, by time series Sentinel-1, Sentinel-2 and Landsat images. Remote Sensing of Environment, 2020, 247, 111951.	11.0	105

#	Article	IF	CITATIONS
19	Mapping paddy rice planting area in rice-wetland coexistent areas through analysis of Landsat 8 OLI and MODIS images. International Journal of Applied Earth Observation and Geoinformation, 2016, 46, 1-12.	2.8	103
20	Rebound in China's coastal wetlands following conservation and restoration. Nature Sustainability, 2021, 4, 1076-1083.	23.7	103
21	The Impact of Urban Renewal on Land Surface Temperature Changes: A Case Study in the Main City of Guangzhou, China. Remote Sensing, 2020, 12, 794.	4.0	99
22	Mapping Deciduous Rubber Plantation Areas and Stand Ages with PALSAR and Landsat Images. Remote Sensing, 2015, 7, 1048-1073.	4.0	89
23	Comparison of surface water extraction performances of different classic water indices using OLI and TM imageries in different situations. Geo-Spatial Information Science, 2015, 18, 32-42.	5.3	89
24	Exacerbated grassland degradation and desertification in Central Asia during 2000–2014. Ecological Applications, 2018, 28, 442-456.	3.8	83
25	Gainers and losers of surface and terrestrial water resources in China during 1989–2016. Nature Communications, 2020, 11, 3471.	12.8	81
26	TROPOMI reveals dry-season increase of solar-induced chlorophyll fluorescence in the Amazon forest. Proceedings of the National Academy of Sciences of the United States of America, 2019, 116, 22393-22398.	7.1	78
27	Improved estimates of forest cover and loss in the Brazilian Amazon in 2000–2017. Nature Sustainability, 2019, 2, 764-772.	23.7	71
28	Ecological engineering projects increased vegetation cover, production, and biomass in semiarid and subhumid Northern China. Land Degradation and Development, 2019, 30, 1620-1631.	3.9	71
29	Forest cover maps of China in 2010 from multiple approaches and data sources: PALSAR, Landsat, MODIS, FRA, and NFI. ISPRS Journal of Photogrammetry and Remote Sensing, 2015, 109, 1-16.	11.1	70
30	Mapping tropical forests and deciduous rubber plantations in Hainan Island, China by integrating PALSAR 25-m and multi-temporal Landsat images. International Journal of Applied Earth Observation and Geoinformation, 2016, 50, 117-130.	2.8	69
31	Mapping the dynamics of eastern redcedar encroachment into grasslands during 1984–2010 through PALSAR and time series Landsat images. Remote Sensing of Environment, 2017, 190, 233-246.	11.0	65
32	Assessing consistency of spring phenology of snow-covered forests as estimated by vegetation indices, gross primary production, and solar-induced chlorophyll fluorescence. Agricultural and Forest Meteorology, 2019, 275, 305-316.	4.8	64
33	Northward expansion of paddy rice in northeastern Asia during 2000–2014. Geophysical Research Letters, 2016, 43, 3754-3761.	4.0	63
34	Characterizing the encroachment of juniper forests into sub-humid and semi-arid prairies from 1984 to 2010 using PALSAR and Landsat data. Remote Sensing of Environment, 2018, 205, 166-179.	11.0	61
35	Fingerprint of rice paddies in spatial–temporal dynamics of atmospheric methane concentration in monsoon Asia. Nature Communications, 2020, 11, 554.	12.8	56
36	Mapping paddy rice planting area in wheat-rice double-cropped areas through integration of Landsat-8 OLI, MODIS and PALSAR images. Scientific Reports, 2015, 5, 10088.	3.3	55

#	Article	IF	CITATIONS
37	Mapping forests in monsoon Asia with ALOS PALSAR 50-m mosaic images and MODIS imagery in 2010. Scientific Reports, 2016, 6, 20880.	3.3	49
38	Annual dynamics of forest areas in South America during 2007–2010 at 50-m spatial resolution. Remote Sensing of Environment, 2017, 201, 73-87.	11.0	47
39	Tracking the spatio-temporal change of cropping intensity in China during 2000–2015. Environmental Research Letters, 2019, 14, 035008.	5.2	46
40	Status of land use intensity in China and its impacts on land carrying capacity. Journal of Chinese Geography, 2017, 27, 387-402.	3.9	44
41	Quantifying annual changes in built-up area in complex urban-rural landscapes from analyses of PALSAR and Landsat images. ISPRS Journal of Photogrammetry and Remote Sensing, 2017, 124, 89-105.	11.1	42
42	Examining the short-term impacts of diverse management practices on plant phenology and carbon fluxes of Old World bluestems pasture. Agricultural and Forest Meteorology, 2017, 237-238, 60-70.	4.8	41
43	Spatial-temporal changes of cropland and climate potential productivity in northern China during 1990–2010. Food Security, 2013, 5, 499-512.	5.3	39
44	Mapping paddy rice distribution using multi-temporal Landsat imagery in the Sanjiang Plain, northeast China. Frontiers of Earth Science, 2016, 10, 49-62.	2.1	39
45	Responses of gross primary production of grasslands and croplands under drought, pluvial, and irrigation conditions during 2010–2016, Oklahoma, USA. Agricultural Water Management, 2018, 204, 47-59.	5.6	38
46	Mapping Forest and Their Spatial–Temporal Changes From 2007 to 2015 in Tropical Hainan Island by Integrating ALOS/ALOS-2 L-Band SAR and Landsat Optical Images. IEEE Journal of Selected Topics in Applied Earth Observations and Remote Sensing, 2018, 11, 852-867.	4.9	35
47	Impacts of ecological restoration projects on agricultural productivity in China. Journal of Chinese Geography, 2013, 23, 404-416.	3.9	33
48	Human-Induced Landcover Changes Drive a Diminution of Land Surface Albedo in the Loess Plateau (China). Remote Sensing, 2015, 7, 2926-2941.	4.0	31
49	Temporal consistency between gross primary production and solar-induced chlorophyll fluorescence in the ten most populous megacity areas over years. Scientific Reports, 2017, 7, 14963.	3.3	30
50	Expansion dynamics of deciduous rubber plantations in Xishuangbanna, China during 2000–2010. GIScience and Remote Sensing, 2018, 55, 905-925.	5.9	30
51	Spatiotemporal Consistency of Four Gross Primary Production Products and Solarâ€Induced Chlorophyll Fluorescence in Response to Climate Extremes Across CONUS in 2012. Journal of Geophysical Research G: Biogeosciences, 2018, 123, 3140-3161.	3.0	30
52	Effects of in-situ and reanalysis climate data on estimation of cropland gross primary production using the Vegetation Photosynthesis Model. Agricultural and Forest Meteorology, 2015, 213, 240-250.	4.8	29
53	Estimating aboveground biomass of broadleaf, needleleaf, and mixed forests in Northeastern China through analysis of 25-m ALOS/PALSAR mosaic data. Forest Ecology and Management, 2017, 389, 199-210.	3.2	29
54	Large loss and rapid recovery of vegetation cover and aboveground biomass over forest areas in Australia during 2019–2020. Remote Sensing of Environment, 2022, 278, 113087.	11.0	26

#	Article	IF	CITATIONS
55	Accuracy Assessment and Inter-Comparison of Eight Medium Resolution Forest Products on the Loess Plateau, China. ISPRS International Journal of Geo-Information, 2017, 6, 152.	2.9	25
56	Enhanced gross primary production and evapotranspiration in juniperâ€encroached grasslands. Global Change Biology, 2018, 24, 5655-5667.	9.5	25
57	Semi-natural areas of Tarim Basin in northwest China: Linkage to desertification. Science of the Total Environment, 2016, 573, 178-188.	8.0	22
58	Mapping Annual Forest Cover in Sub-Humid and Semi-Arid Regions through Analysis of Landsat and PALSAR Imagery. Remote Sensing, 2016, 8, 933.	4.0	21
59	Small anomalies in dry-season greenness and chlorophyll fluorescence for Amazon moist tropical forests during El Niño and La Niña. Remote Sensing of Environment, 2021, 253, 112196.	11.0	21
60	Globalâ€Scale Consistency of Spaceborne Vegetation Indices, Chlorophyll Fluorescence, and Photosynthesis. Journal of Geophysical Research G: Biogeosciences, 2021, 126, e2020JG006136.	3.0	21
61	Impacts of juniper woody plant encroachment into grasslands on local climate. Agricultural and Forest Meteorology, 2021, 307, 108508.	4.8	21
62	Canopy and climate controls of gross primary production of Mediterranean-type deciduous and evergreen oak savannas. Agricultural and Forest Meteorology, 2016, 226-227, 132-147.	4.8	19
63	Forest Changes by Precipitation Zones in Northern China after the Three-North Shelterbelt Forest Program in China. Remote Sensing, 2021, 13, 543.	4.0	17
64	Large spatial variation and stagnation of cropland gross primary production increases the challenges of sustainable grain production and food security in China. Science of the Total Environment, 2022, 811, 151408.	8.0	17
65	Estimating site-specific optimum air temperature and assessing its effect on the photosynthesis of grasslands in mid- to high-latitudes. Environmental Research Letters, 2020, 15, 034064.	5.2	16
66	Tracking Reforestation in the Loess Plateau, China after the "Grain for Green―Project through Integrating PALSAR and Landsat Imagery. Remote Sensing, 2019, 11, 2685.	4.0	14
67	Quantifying spatial-temporal changes of tea plantations in complex landscapes through integrative analyses of optical and microwave imagery. International Journal of Applied Earth Observation and Geoinformation, 2018, 73, 697-711.	2.8	13
68	Multi-scale assessments of forest fragmentation in China. Biodiversity Science, 2017, 25, 372-381.	0.6	11
69	Integrated Analyses of PALSAR and Landsat Imagery Reveal More Agroforests in a Typical Agricultural Production Region, North China Plain. Remote Sensing, 2018, 10, 1323.	4.0	10
70	Area extraction and spatiotemporal characteristics of winter wheat–summer maize in Shandong Province using NDVI time series. PLoS ONE, 2019, 14, e0226508.	2.5	9
71	Social institution changes and their ecological impacts in Kazakhstan over the past hundred years. Environmental Development, 2020, 34, 100531.	4.1	9
72	Assessing variability of optimum air temperature for photosynthesis across site-years, sites and biomes and their effects on photosynthesis estimation. Agricultural and Forest Meteorology, 2021, 298-299, 108277.	4.8	8

#	Article	IF	CITATIONS
73	Spatiotemporal Changes of Winter Wheat Planted and Harvested Areas, Photosynthesis and Grain Production in the Contiguous United States from 2008–2018. Remote Sensing, 2021, 13, 1735.	4.0	6
74	Improved estimation of gross primary production of paddy rice cropland with changing model parameters over phenological transitions. Ecological Modelling, 2021, 445, 109492.	2.5	6
75	Natural and semi-natural land dynamics under water resource change from 1990 to 2015 in the Tarim Basin, China. Environmental Research Letters, 2021, 16, 085001.	5.2	5
76	Annual Maps of Forests in Australia from Analyses of Microwave and Optical Images with FAO Forest Definition. Journal of Remote Sensing, 2021, 2021, .	6.7	3
77	Mapping forest in the southern Great Plains with ALOS-2 PALSAR-2 and Landsat 7/8 data. International Journal of Applied Earth Observation and Geoinformation, 2021, 104, 102578.	2.8	3
78	Mapping Panax Notoginseng Plantations by Using an Integrated Pixel- and Object-Based (IPOB) Approach and ZY-3 Imagery. Remote Sensing, 2021, 13, 2184.	4.0	2
79	Difference and uncertainty of forest coverage estimation in China. Biodiversity Science, 2015, 23, 830-834.	0.6	2
80	Reply to: "Correlation between paddy rice growth and satellite-observed methane column abundance does not imply causation― Nature Communications, 2021, 12, 1189.	12.8	1
81	Title is missing!. , 2019, 14, e0226508.		0
82	Title is missing!. , 2019, 14, e0226508.		0
83	Title is missing!. , 2019, 14, e0226508.		0
84	Title is missing!. , 2019, 14, e0226508.		0
85	Title is missing!. , 2019, 14, e0226508.		0
86	Title is missing!. , 2019, 14, e0226508.		0